Influence of the gap size on the wind loading on heliostats

Cite as: AIP Conference Proceedings **1734**, 020019 (2016); https://doi.org/10.1063/1.4949043
Published Online: 31 May 2016

Pierre E. Poulain, Ken J. Craig and Josua P. Meyer

Influence of the Gap Size on the Wind Loading on Heliostats

Pierre E. Poulain[1], Ken J. Craig[2,a)] and Josua P. Meyer[2]

[1]*PhD student,* [2]*PrEng PhD, Professor*
Department of Mechanical and Aeronautical Engineering, University of Pretoria, Pretoria 0002, South Africa.

[a)]Corresponding author: ken.craig@up.ac.za.

Abstract. Generally built in desert areas, heliostat fields undergo various wind loading conditions. An ANSYS Fluent CFD model of an isolated heliostat in worst-case orientation for the drag force is realized via numerical simulations using the realizable k-ε turbulence model. This paper focuses on the gap width between the panels and its influence on the wind loading that heliostats are subjected to. An atmospheric boundary layer profile is generated based on a wind tunnel experiment. For a heliostat in upright and tilted orientations with the wind angle being zero degrees, the gap width is varied and the force and moment coefficients are calculated. In the range tested, all the coefficients globally increase with the widening of the gaps.

INTRODUCTION

The heliostat field of a solar tower power station represents from 30 to 50% of its total capital cost. In terms of profitability, it is therefore important to investigate improvements in the design of heliostats so that the field is built at a lower cost or renders a higher optical efficiency. For that reason, it is essential to find methods that reduce the wind loading over the heliostat structure. Recent wind tunnel experiments show the beneficial effects of an individual porous wind protection device on a light-weight heliostat [1] and wind fences surrounding the field [2]. The effect of introducing gaps between the panels constituting the reflector has been addressed but only to a certain extent: small gaps along the two directions of the mirror [3] and one median wide gap along the heliostat chord direction [4].

NOMENCLATURE

A	Reflector area (m^2)	L	Heliostat characteristic length (m)
ABL	Atmospheric boundary layer	*l*	Panel width (mm)
C_F	Force coefficient	M	Wind induced moment (N.m)
C_M	Moment coefficient	u^*_{ABL}	Friction velocity of the atmospheric boundary layer (m/s)
CFD	Computational Fluid Dynamics	z_0	Aerodynamic roughness length (m)
e	Gap width (mm)	α	Heliostat elevation angle (º)
F	Wind induced force (N)	β	Wind angle (º)
G_r	Gap-to-mirror surface area ratio	ε	Turbulence dissipation rate (m^2/s^3)
I_u	Streamwise turbulence intensity (%)	κ	von Karman contant
k	Turbulent kinetic energy (m^2/s^2)	ρ	air density (kg/m^3)

Even though wind tunnel tests are preferred for heliostat design, Computational Fluid Dynamics (CFD) provides valuable information for the design and optimization of a heliostat structure and can give a fairly good agreement with experimental results [3]. Moreover, it delivers a good representation of the flow field all around the models whilst wind tunnel tests are limited to measured data sets. Another advantage of CFD is the possibility to explore many various designs before building a model that undergoes wind tunnel tests. The number of CFD studies

SolarPACES 2015
AIP Conf. Proc. 1734, 020019-1–020019-9; doi: 10.1063/1.4949043
Published by AIP Publishing. 978-0-7354-1386-3/$30.00

covering the wind loading on heliostats remains however low. Most heliostat designs present gaps in between the facets as it is easier to manufacture and allows for the use of standard mirror sizes. It has thus been decided to pursue with the investigation of gap size effect on the wind loading.

The heliostats are mostly tracking the sun by rotating about two axes, namely azimuthal and elevation. They are actuated with two drive mechanisms which constitute about one third of a heliostat capital cost [5]. The drives of a lighter heliostat will undergo more stresses due to wind loading. It is therefore important to explore ways to keep the wind loads to a minimum. The current study investigated the possibility of altering the shape of the larger circulation bubble in the heliostat wake through the creation of smaller recirculation zones. Peterka and Derickson [6] as well as Wu et al. [3] concluded that creating openings in the mirror area has a small effect on the wind loading if they represent less than 15% of the mirror area. However, there is no estimation in the open literature for greater gap areas which is the focus of this study.

CFD MODEL SET-UP

Geometry

The aim of the study is to replicate a wind tunnel test of Peterka et al. [7] with an ANSYS Fluent V15.0 CFD model with slight variations of the original geometry (Fig. 1a), namely the gap width between panels. The width of a panel is 35.6mm for a chord of 10.82cm. Therefore, the aspect ratio is 1.08 if accounting for the gaps having a width of about e=5.1mm. The height of centreline i.e. the pylon length is 6.86cm. An alternative coordinate system has been employed (Fig 1b).

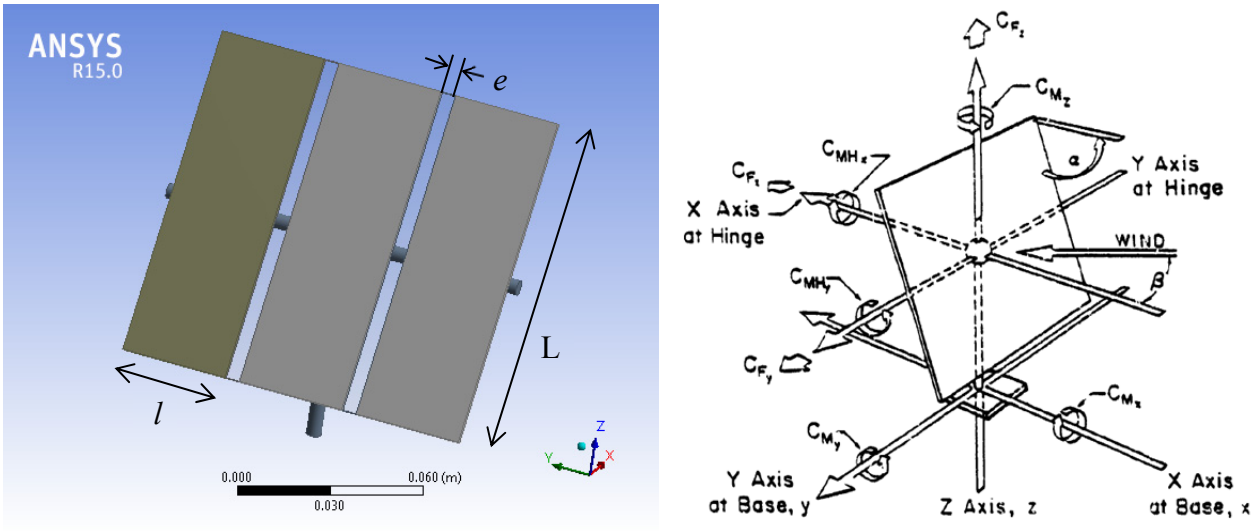

(a) (b)

FIGURE 1. (a) Heliostat model and (b) coordinate system from [6]

Inlet Profiles

A heliostat structure is subjected to an atmospheric boundary layer profile which is not uniform. An accurate CFD model of the wind flow around a heliostat requires modeling of the appropriate boundary conditions. Ideally, to replicate the inlet profile, one should model the presence of ground elements upstream the heliostat model. However, this would require high upstream length and high number of cells. In order to address the computational cost issue, used fully developed profiles generated at reasonable distance upstream of the heliostat model are used. Richards and Hoxey [8] derived a set of equations (1) for the k-ε model based on three main assumptions (no

vertical velocity, constant pressure and constant shear stress) in order to achieve a horizontally homogeneous ABL profile. The ABL friction velocity can be calculated using reference values for height and velocity.

$$U(z) = \frac{u^*_{ABL}}{\kappa}\ln\left(\frac{z}{z_0}\right),\ \mathrm{k} = \frac{u^{*\,2}_{ABL}}{\sqrt{C_\mu}},\ \varepsilon = \frac{u^{*\,3}_{ABL}}{\kappa} \tag{1}$$

The aerodynamic roughness length, z_0, represents the height of roughness elements on the ground. One can play around with this parameter to change the inlet profiles. In fact, an increase will result in a lower mean velocity but higher turbulence intensity. It has been experimentally shown that results are highly sensitive to the turbulence intensity level [9]. For that matter, we aimed to obtain a fairly good match of the turbulence intensity inlet profile we generate in the CFD model with the experimental one extracted in [7]. The mean velocity may be under or over predicted as long as it stays in the range of Reynolds number independency for the pressure coefficients (10^4-10^5 at model scale) [7]. Under the assumption of isotropic turbulence, the turbulence intensity is calculated with equation (2):

$$I_u(z) = \frac{\sqrt{\frac{2}{3}k}}{U(z)} \tag{2}$$

Since turbulence dissipates near the walls, it is crucial to verify that the profiles are maintained throughout the domain. Indeed, if this is not addressed, both turbulence intensity and mean velocity profile changes as the flow travels up to becoming uniform which may produce unreliable results. Blocken et al. [10] explored several ways to prevent this. One of them is to apply a wall shear stress on the ground (see equation 3). Figure 2 shows the effect of applying such a wall shear stress compared to a standard no-slip condition.

$$\tau_w = \rho u^{*\,2}_{ABL} \tag{3}$$

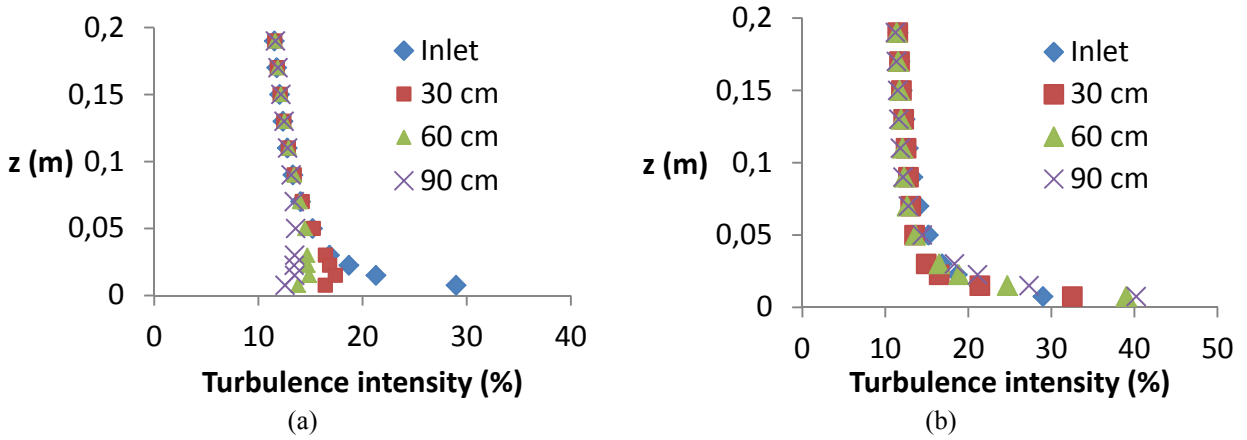

FIGURE 2. Evolution of the turbulence intensity profile as fluid travels through the domain: without shear stress (a) and with shear stress (b) applied to the ground wall

Previous studies pointed out the difficulty to have matching profiles with wind tunnel tests [11]. Specifically, if one decides to have the best match for the mean velocity profile, the turbulence intensity profile will be of lower magnitude. For this study, it has been decided to match the turbulence intensity profile as much as possible playing on the aerodynamic roughness length. Hence, with z_0=7.10^{-4}m, the turbulence intensity profiles are fairly close to one another the zone of interest (Fig. 2b), the height of centreline being at about $\frac{z}{z_{ref}} = 0.06$. Moreover, the mean velocity profiles offer a good match (Fig. 2a). In fact, the mean velocity profile is not as sensitive to the aerodynamic roughness length as the turbulence intensity profile is.

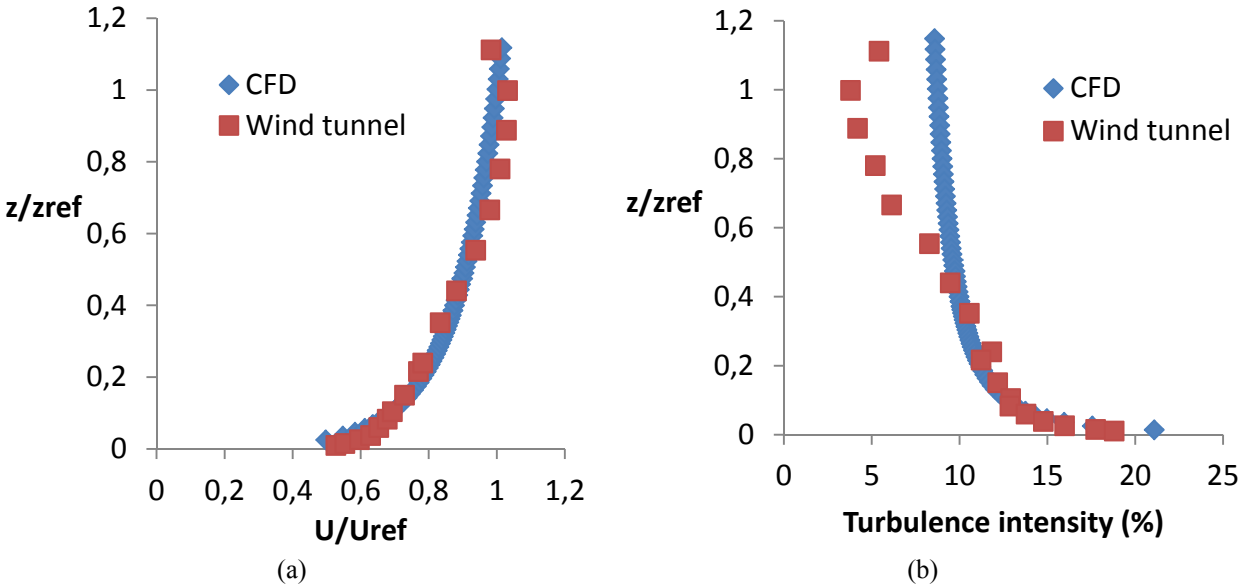

FIGURE 3. Inlet mean velocity profiles (a) and turbulence profiles (b) for the CFD model and Peterka et al.'s experiment

Computational Domain

The cross section of the domain is 2.05x1.83m^2 (approximately the same as Colorado State University's wind tunnel utilized by Peterka et al. [7, 9]). The model is placed 0.75m downstream of the inlet boundary and does not provoke any blockage effect (which would result in an over-prediction of the wind loads) and the total length of the domain is about 6m, enabling the visualization of the entire wake generated downstream of the heliostat. The CFD model includes mesh interfaces (Fig. 4) in order to decrease the computational costs. The area of interest around the heliostat is meshed with tetrahedrons, more convenient for sharp edges and round shapes, whereas the rest of the domain is subdivided by hexahedrons (Fig. 4). The number of cells ranged from 7 million to 12 million depending on the gap width.

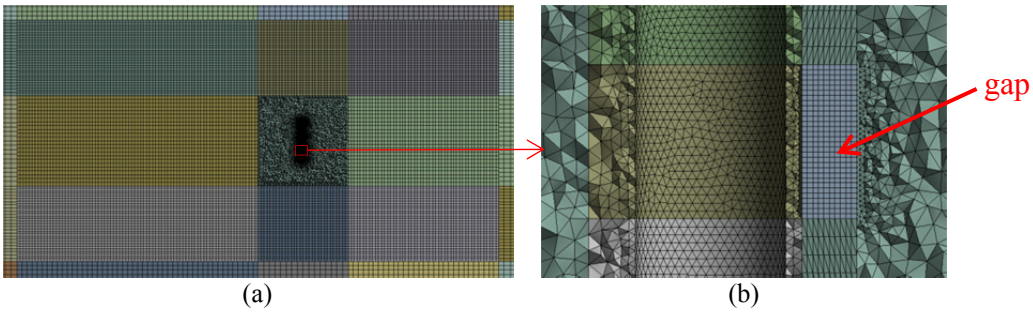

FIGURE 4. View of the mesh in x-y plane (a) and close-up around a gap (b)

Boundary Conditions

In order to replicate Peterka et al.'s wind tunnel test [7], the side and top walls are set to a zero-shear stress boundary condition. To address the decay of the inlet profiles, a shear stress, given by equation (3) is applied on the ground wall that is upstream the heliostat model. The rest of the ground wall and the model satisfy the no-slip condition. The exit of the domain is given a pressure outlet condition. The velocity inlet generates the profiles by means of a User-Defined Function containing equation (1). The reference velocity at z=0.167m is 12.2m/s. All the simulations of the turbulent flow past the heliostat model utilize the realizable version of the k-ε model with enhanced wall treatment.

VARIATION OF GAP WIDTH

Validation

The force and moment coefficients are computed using equation (4) where U is the free-stream velocity at z=0.167m. Note that C_{My} refers to the hinge moment coefficient generally expressed as C_{MHy}. In [7], the reference area comprises the gaps. This is also the case, here, for a gap width equal to that in [7]. When the gap width is varied, the reference area remains the same so that differences in terms of wind loading are possibly noticed.

$$C_{Fx,y,z} = \frac{F_{x,y,z}}{\frac{1}{2}\rho U^2 A}, \quad C_{Mx,y,z} = \frac{M_{x,y,z}}{\frac{1}{2}\rho U^2 AL} \tag{4}$$

The orientations presenting the worst case for the drag (α=90º, β=0º) and lift (α=30º, β=0º) forces are simulated and results are compared with Peterka et al. [7] (Table 1).

Table 1. Comparison of CFD to experimental values

α	β	Coefficient	Experiment [7]	CFD	Error
90º	0º	C_{Fx}	1.26	1.025	-18.7%
30º	0º	C_{Fz}	0.80	0.683	-14.6%
30º	0º	C_{My}	0.13	0.097	-25.4%

Although the difference with the experimental data is rather consequent, the aim is to notice any change in the coefficients with a widening of the gaps. The flow field distribution (Fig. 5) given by the CFD simulations is similar to the one observed in other CFD studies [3, 12].

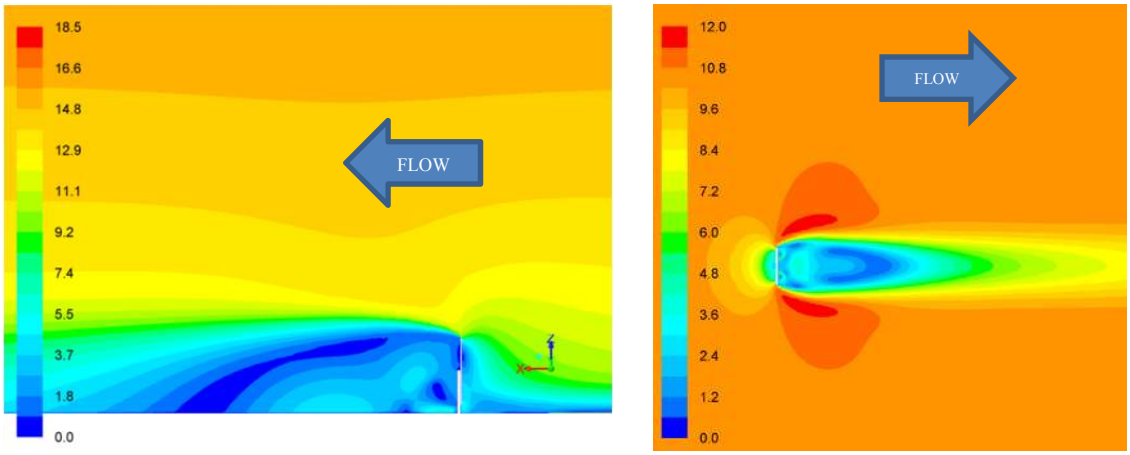

(a) (b)

FIGURE 5. Contours of velocity magnitude (m/s) (α=90º, β=0º) in (a) z-x plane and (b) x-y plane

Results

The parameter of interest is the gap-to-mirror surface area ratio which is defined by equation (5) with parameters presented in Fig. 1a. Its value ranges from about 10% to 50% in this study. One can see on Figure 6 the difference between a ratio of 9.5% and 32.8%. Results for the upright position (α=90º, β=0º) and a tilted orientation (α=30º, β=0º) are presented here.

$$G_r = \frac{2e}{3l} \tag{5}$$

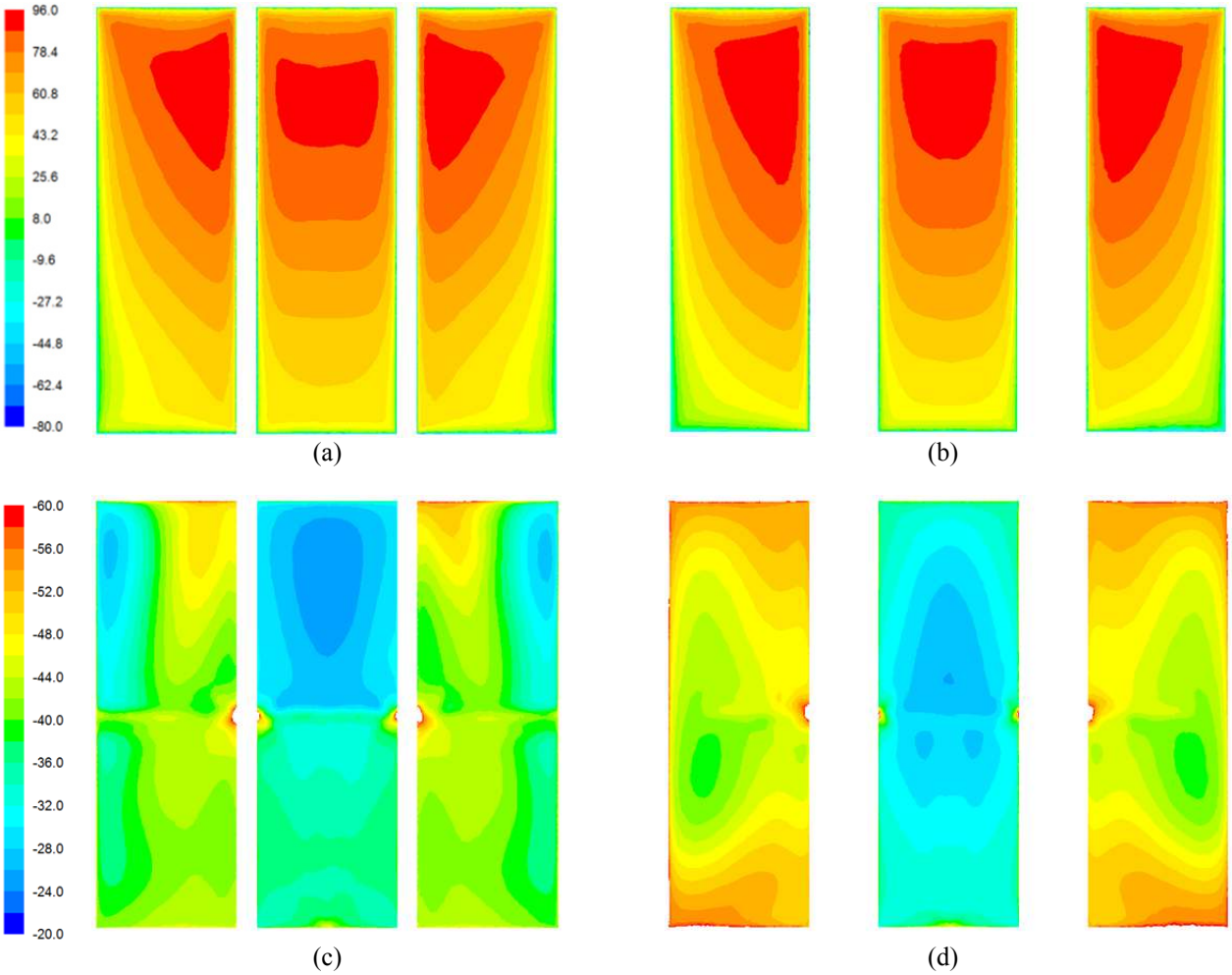

FIGURE 6. Pressure contours on front face for (a) G_r=9.5% and (b) G_r=32.8% and back face ((c) and (d)) for an upright orientation (α=90º, β=0º)

As one can see on Figure 6, the pressure becomes greater on the higher part of the front face and lower on its lower part. This has the effect of moving up the center of pressure and increase the hinge moment. Regarding the back face of the heliostat, not only the static pressure globally increases (Fig. 6c and 6d), the contours pattern also changes due to the conflict between the backflow in the wake and the flow coming through the gaps. With the widening of the gaps, the effective bluff-body area increases which causes the drag force to rise as well.

Figure 7 shows in what order the drag force and hinge moment coefficients increase as the gaps are increased. For instance, if starting with the original dimensions of the heliostat model used for Peterka et al.'s wind tunnel test [7] (e=5.1mm, G_r=9.5%), widening the gaps to a width of 15mm (i.e. G_r=28.1%) raises the drag force coefficient by 4% and the hinge moment coefficient by 26%.

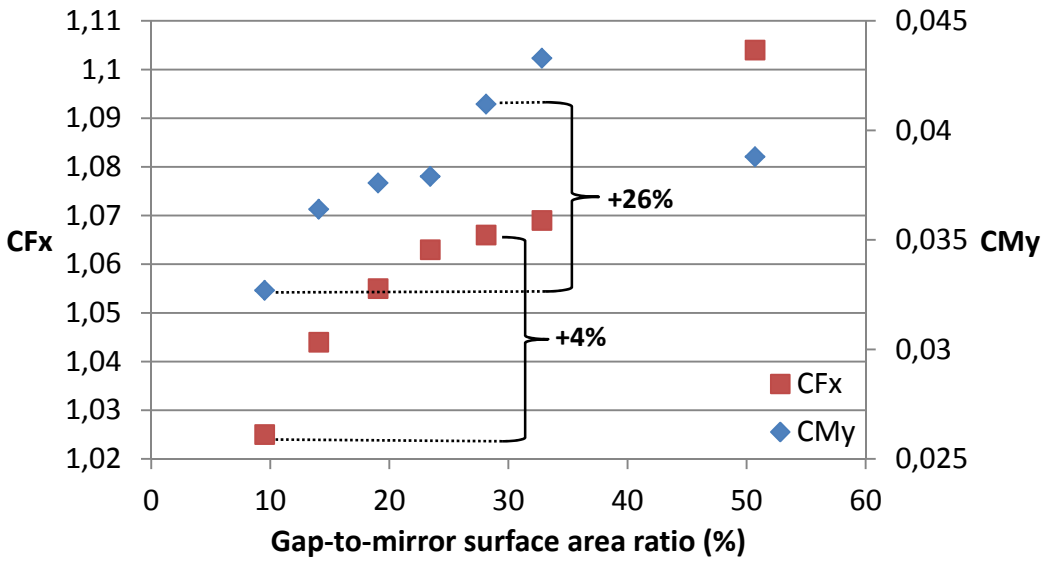

FIGURE 7. Evolution of the drag force (red) and hinge moment (blue) coefficients as the gap width changes (α=90º, β=0º)

When looking at the vectors of the velocity coloured by pressure (Fig. 8), we observe that widening the gaps favours the emergence of a second recirculation zone between the gaps and the edges of the heliostat.

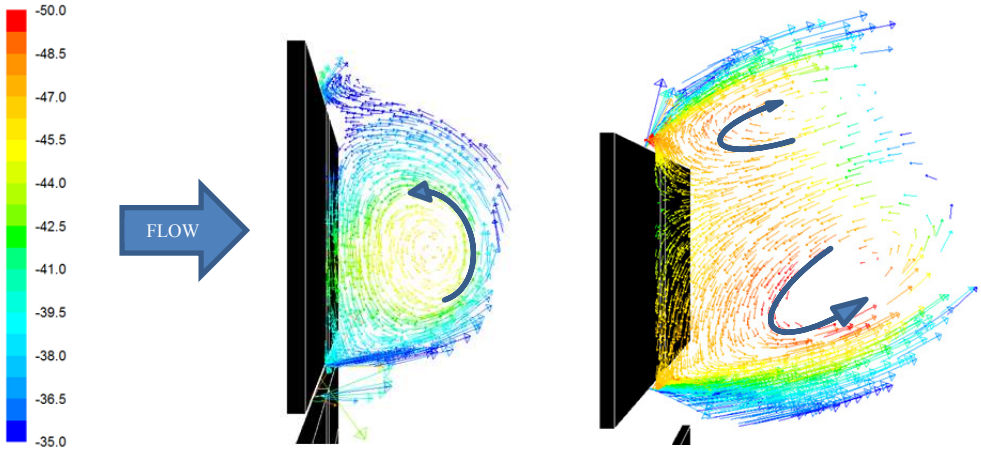

FIGURE 8. Vectors of velocity coloured by static pressure behind a side panel in x-y plane for (a) G_r=9.5% and (b) G_r=32.8% (α=90º, β=0º)

Moreover, the two recirculation zones show lower velocities for higher static pressures in terms of absolute value (Fig. 7).

Figure 9 presents the results for a tilted heliostat (α=30º, β=0º). They present the same trend: as the gap width increases, the coefficients rise. Whereas for the upright case only the drag coefficient (C_{Fx}) and hinge moment were displayed, we now also have a lift coefficient (C_{Fz} in Fig. 9b) for this tilted orientation. The influence of widening the gaps up to G_r=32.8%, results in an increase for C_{Fx}, C_{Fz} and C_{My} of 9%, 4% and 6%, respectively.

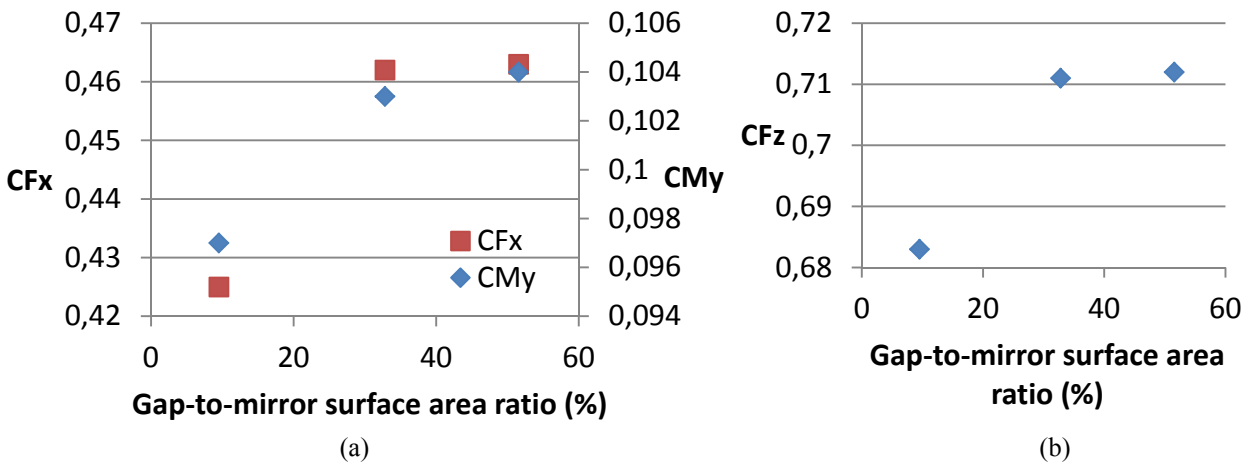

(a) (b)

FIGURE 9. Evolution of (a) the drag force (red) and hinge moment (blue) and (b) the lift force coefficients as the gap width changes (α=30º, β=0º)

The flow that travels through wide gaps has more weight in the establishment of the flow distribution in the wake of the structure. It actually increases the static pressure in the recirculation zones (Fig. 10) and therefore increases the global loading over the heliostat model.

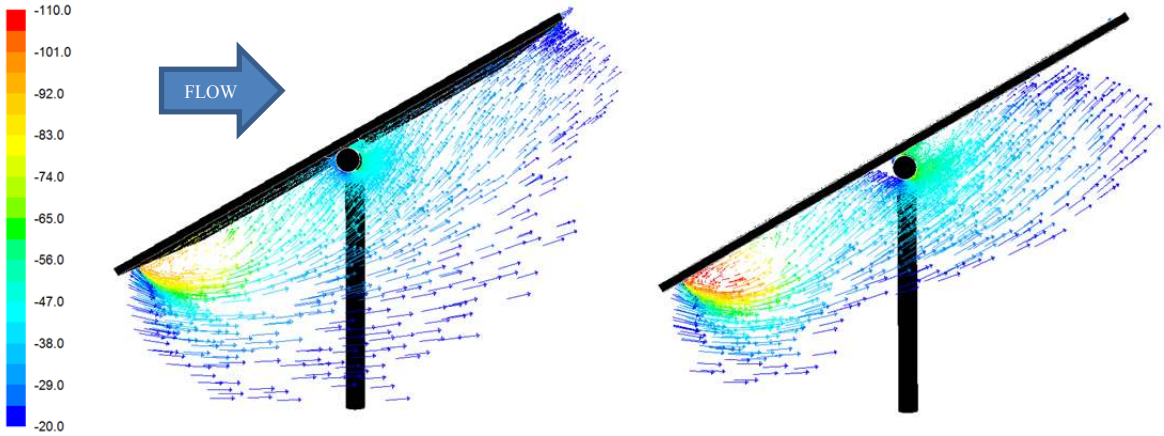

(a) (b)

FIGURE 10. Vectors of velocity coloured by static pressure behind a side panel in x-y plane for (a) G_r=9.5% and (b) G_r=32.8% (α=30º, β=0º)

CONCLUSION

In order to model the ABL, due to the coupling between mean velocity and turbulence intensity, it is preferable to set a value for the aerodynamic roughness length that gives the level of turbulence intensity desired rather than the mean velocity profile. Applying a shear stress based on the ABL friction velocity is efficient for maintaining the inlet profiles as the fluid travels through the domain.

For a heliostat with two gaps parallel to its chord orientated such that the drag force or the lift force is maximum, having wider gaps between the panels is not beneficial in terms of wind loading since this increases the drag and lift force coefficients as well as the hinge moment coefficient.

Further studies are needed regarding other heliostat orientations and heliostat designs. In this study, the gaps are parallel to the heliostat chord. A different trend could be expected if these are perpendicular to the chord instead or if there is only one central gap.

ACKNOWLEDGEMENT

The authors would like to acknowledge the support from the University of Pretoria (South Africa) and the South African National Research Foundation (DST-NRF Solar Spoke).

REFERENCES

1. A. Pfahl, A. Brucks and C. Holze, “Wind load reduction for light-weight heliostats”, in SolarPACES 2013, Elsevier: Las Vegas.
2. H. Liu, B. Gong, Z. F. Wang and Z. N. Li, “Wind tunnel studies of wind fences for reduction of wind flow and wind loads on heliostat”, in SolarPACES 2014, Elsevier: Beijing.
3. Z.Wu, B. Gong, Z. Wang, Z. Li and C. Zang, Renewable Energy, 2010, 35: p. 797-806.
4. A. Pfahl, M. Buselmeier and M. Zaschke, “Determination of wind loads on heliostats”, in SolarPACES 2011, Elsevier: Granada.
5. A. Pfahl, Journal of Solar Energy Engineering, Vol. 136 (1), 2013.
6. J. A. Peterka, and R. G. Derickson, “Wind load design methods for ground-based heliostats and parabolic dish collectors”, Sandia National Laboratories: Springfield, Alabama, USA, September 1992.
7. J. A. Peterka, N. Hosoya, B. Bienkiewicz, and J. E. Cermak, “Wind load reduction for heliostats”. Technical Report for Solar Energy Research Institute, Solar Energy Research Institute, USA, May 1986.
8. P. J. Richards and R. P. Hoxey, Journal of Wind Engineering and Industrial Aerodynamics, 1993. 46: p. 145-153.
9. J. A. Peterka, Z. Tan, B. Bienkiewicz and J. E. Cermak, “Mean and peak wind load reduction on heliostats”, Technical Report for Solar Energy Research Institute, September 1987.
10. B. Blocken, T. Stathopoulos and J. Carmeliet, Atmospheric environment, 2007. 41(2): p. 238-252.
11. M. D. Marais, K. J. Craig and J. P. Meyer, “Computational flow optimization of heliostat aspect ratio for wind direction and elevation angle”, in SolarPACES 2014, Elsevier: Beijing.
12. Y. Wang and L. Zhengnong, Key Engineering Materials, Vol. 517, 2012, pp 809-816.